

Effect of Silicon and Retained Austenite on the Liquid Metal Embrittlement Cracking Behavior of GEN3 and High-Strength Automotive Steels

The effect of silicon on the liquid metal embrittlement cracking behavior of 980-MPa GEN3 automotive steels is explained through weldability evaluations and Gleeble® simulations. The role of retained austenite in LME cracking is clarified

BY M. TUMULURU

ABSTRACT

GEN3 steels are a new family of automotive sheet steels developed and commercialized in the last three years. specifically for body-in-white applications. The high ductility in GEN3 steels is typically achieved through the transformation-induced plasticity (TRIP) effect by the addition of silicon or aluminum. When these steels are formed into parts, the TRIP effect of austenite to martensite transformation provides enhanced ductility. Typically, 10 to 12 micrometers of zinc coating (known as galvanized coating) is applied to automotive steel sheets for corrosion protection. Liquid metal embrittlement (LME) cracking can occur during resistance spot welding (RSW) of galvanized steels. LME cracking occurs when molten zinc penetrates prior austenite grain boundaries of the steel substrate. The precise role of silicon in the LME cracking behavior in TRIP and GEN3 steels is unknown. Therefore, a study was undertaken to examine the role of silicon in LME cracking behavior of GEN3 steels. The purpose was also to examine if the presence of retained austenite is required for LME cracking to occur. In this study,

laboratory heats were prepared using three silicon levels. Samples cut from galvanized panels were welded using a resistance spot welding machine, and weld areas were examined metallographically for the presence of LME cracks. Gleeble® simulations were done to study the LME behavior of the three steels prepared. Base materials were examined with a scanning electron microscope using the electron backscattered diffraction (EBSD) method to examine the nature of grain boundaries found. The effect of retained austenite in LME cracking was studied using the Gleeble®. Both RSW and Gleeble® results showed silicon promotes LME cracking in steels, predominantly in the weld heat-affected zones (HAZs). More low-energy, low-coincidence site lattice (CSL) boundaries were found as the silicon content of the steel was decreased. These boundaries do not host cracks. Higher silicon appeared to shrink the safe temperature range over which LME cracks could be avoided, thus indicating heat input control to limit cracks has limited windows as the silicon in steel goes up. It was shown that the presence of retained austenite in steel is not a prerequisite for LME cracking to

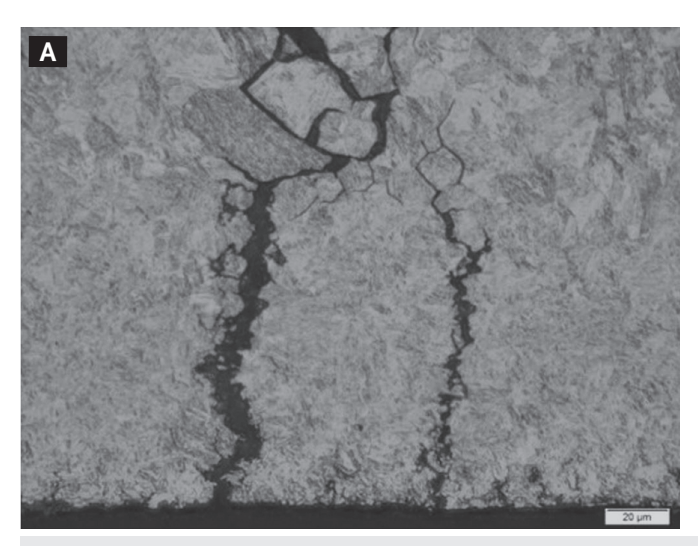
KEYWORDS

- Resistance Spot Welds LME Cracking GEN3 Steels
- Gleeble[®] Silicon Electrogalvanized
- Retained Austenite

Introduction

A new generation of sheet steels, termed GEN3 steel, was developed and commercialized in the last three years for body-in-white applications in the automotive industry (Ref. 1). GEN3 steels are so named to distinguish them from GEN1 and GEN2 steels. GEN1 steels include dual-phase and transformation-induced plasticity (TRIP) steels. GEN2 steels include such steel grades as twinning-induced plasticity (TWIP) steels and austenitic steels. GEN1 steels possess

excellent weldability and have been in commercial use for nearly two decades (Ref. 2). The goal in developing GEN3 steels was to commercialize steels that have higher strength and elongation than GEN1 steels and have better weldability and lower cost than GEN2 steels. GEN2 steels have limited global availability, and so have found limited applications. While there is no standard definition for what strengthelongation properties constitute a GEN3 steel, it is proposed that when the product of strength (in MPa) and elongation (in percent) equals or exceeds 20,000 MPa-percent, the steel falls under the GEN3 category. Modifications to processing and compositions to have small amounts of retained austenite in the steel have enabled the introduction of a new category of steels in the GEN1 family called GEN1 Plus steels. These steels have strength-elongation product equal to or greater than 15,000 MPa-percent.



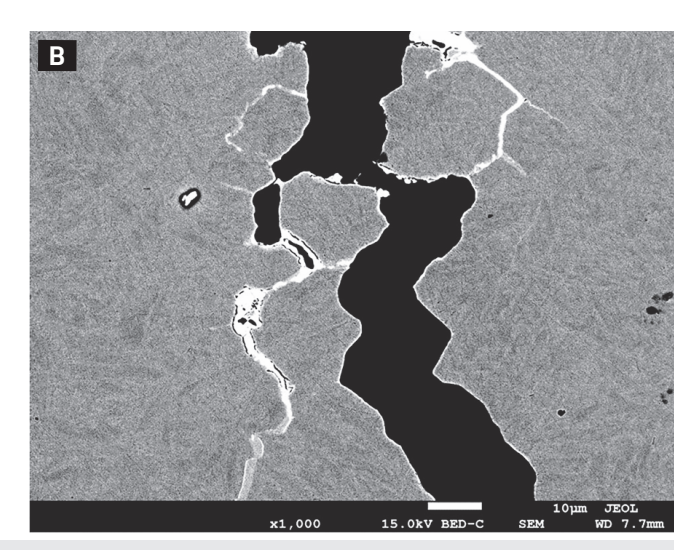


Fig. 1 — Typical LME cracks seen in steels. A — Optical view; B — SEM view.

It is possible to attain the required properties for GEN3 steels by taking advantage of the TRIP-effect, which is strain-induced transformation of austenite to martensite. Generally, 980-MPa GEN3 steels contain between 15 and 20% retained austenite to achieve the required strengthelongation properties. Austenite is stabilized and enriched with carbon by retarding the formation of carbides. Two elements that can effectively do this are silicon and aluminum. The advantage of silicon over aluminum is that it provides additional strengthening through a solid-solution mechanism, thereby reducing the need to add a large amount of carbon to achieve high strength. Carbon is not a preferred element in steel as increasing carbon can cause weldability issues. Carbon has a strong influence on what is known as "carbon equivalent" (CE) in steels, whereas silicon has only a lower effect in increasing CE (Ref. 3). Steels with higher CE require additional precautions to achieve satisfactory quality welds. GEN3 steels are typically produced through the quench and partition method, a process described in Refs. 4 and 5.

Steels used in body-in-white applications have a thin layer of zinc applied on them prior to supply. The zinc layer can be applied using an electrolytic plating (electrogalvanizing) process. These plated steels are welded in automotive applications predominantly using the resistance spot welding (RSW) process. Resistance welding of zinc-coated steels can cause liquid metal embrittlement (LME) cracking in welds. Liquid metal embrittlement is a phenomenon that occurs in steels when the steel substrate under tension is exposed to certain embrittling liquid metals, such as copper or zinc. During welding, molten copper or zinc can penetrate into the grain boundaries of the steel substrate and lower the



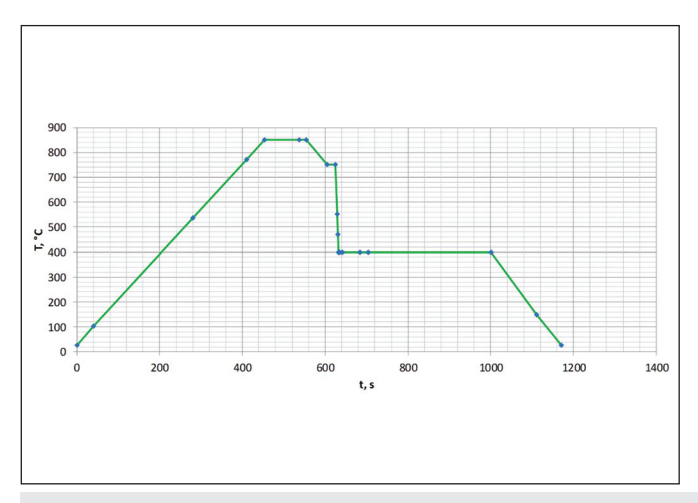
Fig. 2 — A view of the CAL simulator. It is equipped with an IR furnace featuring slow cooling capability, rapid cooling zone, and a quench tank.

substrate ductility and also induce cracking. Cracking has typically been observed to occur along prior austenite grain boundaries in steel — Fig. 1.

Three prerequisites are required for LME cracking to occur in steels. These include the presence of liquid metal of the embrittling type (copper or zinc), the presence of tensile stress, and a susceptible microstructure. All these conditions are present in RSW of galvanized high-strength steels. Wettability of the substrate by the molten metal is an important factor for LME cracking to occur. If the molten metal does not wet the substrate, then penetration of molten zinc into

Table 1 —	Chemical Co	nmnositions	(wt-%) of	the Three Heats
I UDIC I	Olicillicat o		LAAC 101 OI	tile illice ileuts

Heat	С	Mn	Р	S	Si	Cu	Ni	Cr	Мо
Α	0.244	2.231	0.0081	0.0022	0.399	0.0110	0.0057	0.0398	0.0007
В	0.257	2.245	0.0086	0.0021	0.903	0.0110	0.0056	0.0397	0.0009
С	0.245	2.217	0.0083	0.0019	1.357	0.0107	0.0053	0.0391	0.0007



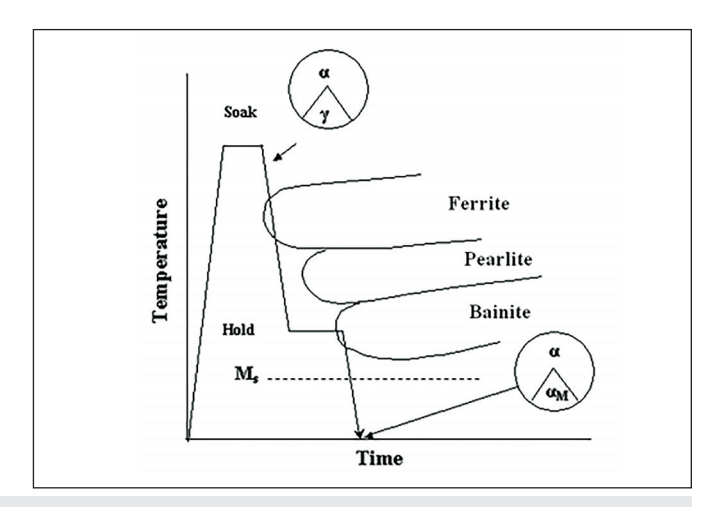


Fig. 3 — A profile of the heat treatment cycle in the CAL simulator is shown in the left figure. A schematic of the heat treatment typically used to produce TRIP steels is shown on the right.

Table 2 — Welding Equipment Details

Welding Machine Manufacturer Welding Machine Type **Welding Machine Transformer** Welding Controller **Electrode Coolant Water** Temperature Tip Cooling Water Flow Rate

Taylor Winfield Corp. Pedestal Type 100 kVA Miyachi (constant current type) 21°C

3.7 L (1 gal)/min

the steel substrate can be eliminated. However, any additions or changes to the zinc coating to prevent wetting during welding can cause poor coating adhesion of zinc during galvanizing. Liquid metal embrittlement cracking in steels has been researched since the 1970s starting with Stoloff and co-workers at RPI (Refs. 6, 7). More recently, Beal and co-workers, as well as Kang and their co-workers, studied LME cracking as it applies to TWIP steels (Refs. 8, 9). Liquid metal embrittlement cracking in welds in TRIP and other advanced high-strength steels has been reported by many (Refs. 10–14). Several models have been proposed to explain the LME phenomenon. Some salient ones include the adsorption-induced reduction in cohesion (Stoloff, Johnson, Westwood, and Kamdar), stress-assisted dissolutiondiffusion (Robertson and Glickman), and surface energy reduction (Rostoker and Rehbinder). A summary of these models and their principal features are provided in Ref. 9.

Most of these studies have focused on understanding the mechanism involved in the LME phenomenon and the factors that can affect cracking in resistance spot welds. These studies were focused on GEN1 and GEN2 steels that included TWIP and TRIP steels. With the introduction of GEN3 steels for automotive use, it is important to examine and understand the LME cracking behavior of these steels. Considering the similarities between GEN3 steel and TRIP steel in microstructural constituents and composition, the LME study of GEN3 steel becomes all the more important. This is because galvanized 780-MPa TRIP steel was reported to ex-

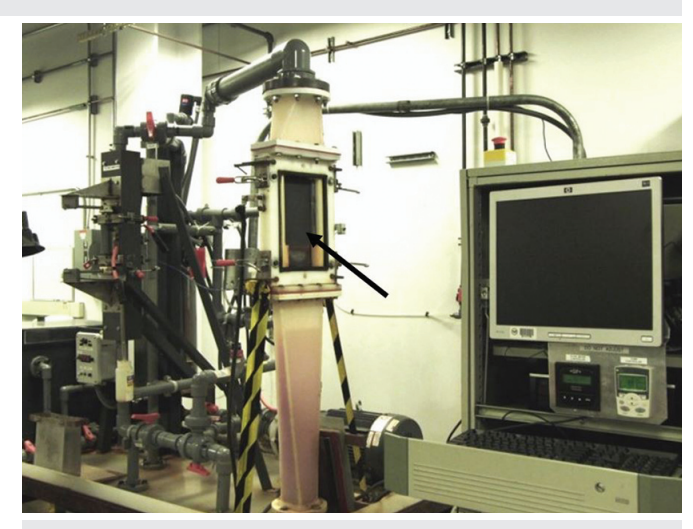


Fig. 4 — Laboratory electrolytic recirculating cell used for electrogalvanizing samples. Arrow shows sample panel location for electrogalvanizing.

hibit LME cracking (Ref. 15). Studies were published on the effect of LME cracks on the strength of welds in GEN1 steels (Refs. 16, 17). There have not been many studies reported on the weldability or LME behavior of GEN3 steels. Among those few LME studies on GEN3 steel, the effect of coating weight on LME cracking and comparison of different hotdip coatings have been reported in Refs. 18 and 19.

GEN3 steels typically contain high silicon to suppress carbide precipitation during heat treatment and stabilize retained austenite for ductility enhancement. Neither the effect of silicon nor retained austenite in the LME behavior of steel has ever been reported before. Further, there is a prevailing notion in the automotive industry, which has not been investigated so far, is that steels containing retained austenite are prone to LME cracking. Therefore, a fundamental study using laboratory heats was undertaken to examine the effect of silicon on the LME cracking behavior of resistance spot welds in these steels. The aim was also to clarify the role of retained austenite in the occurrence of LME cracks. Both resistance spot welds and Gleeble® exami-

WELDING RESEARCH



Fig. 5 — Photograph of a Gleeble® sample used.

Table 3 — Welding Conditions Used

Electrode Face Diameter	6.09 mm
Electrode Force	3.6 kN
Electrode Tip Geometry	Double Dome
Squeeze Time	80 cycles
Weld Time	14 cycles
Hold Time	10 cycles
Preheating	None
Postheating	None

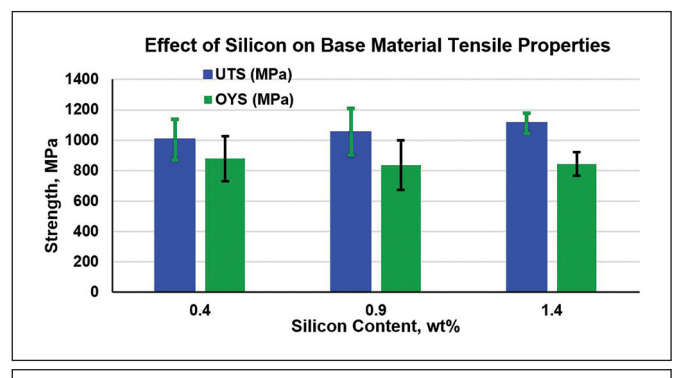
Table 4 — Results of Retained Austenite Determination

Si Content, wt-%	Retained Austenite, percent
0.4	<1
0.9	8
1.4	8.9

nations were used in this study to examine the roles of silicon and only Gleeble® was used to study the influence of retained austenite. Welding studies to examine LME cracking behavior is important as welds are subject to unique rapid heating involving melting and rapid cooling, and are simultaneously subject to tensile and compressive stresses. Further, the use of welding to study LME cracking behavior of welds makes comparison of weld cracking data with those of Gleeble® results possible.

Materials and Experimental Procedure

One split heat was melted in a vacuum induction furnace weighing about 135 kg, with three 45-kg ingots, each measuring $75 \times 200 \times 350$ mm cast. The three split ingots were made with three silicon levels. The compositions of the three heats cast are shown in Table 1. The compositions of all heats except for silicon levels are typical of 980-MPa GEN3 steels. The ingots were hot rolled to 4 mm. They were then surface ground to 2.5 mm before cold rolling, thereby removing nearly 0.7 mm per side. The surface grinding removed any surface and subsurface oxides present in the hot bands and eliminated the need for pickling to remove mill scale. The 2.5-mm hot bands were cold rolled to a final thickness of 1.2 mm. Panels measuring 250 × 170 mm were cut from the cold rolled material for heat treatment in a continuous annealing (CAL) simulator. A CAL simulator can simulate the heat treatment cycles used in a typical CAL line, and is helpful for producing laboratory panels for study. The heat treatment was done in a ULVAC CAL, which is



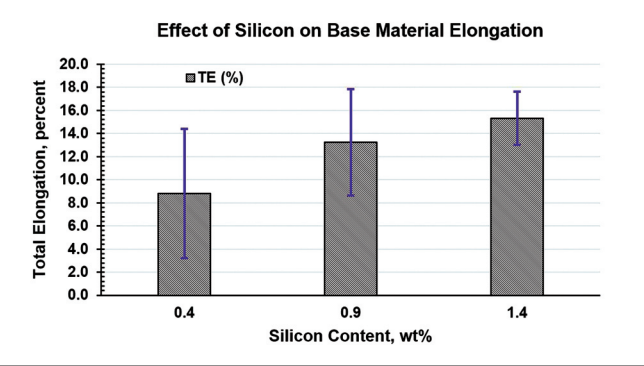


Fig. 6 — Effect of silicon on the strength and elongation of the base materials.

shown in Fig. 2.

The heat treatment cycle followed is shown in Fig. 3. This represents a typical heat treatment cycle to produce TRIP steels and had an annealing soak temperature of 850°C, with an overaging cycle at 450°C. A Q&P cycle typically used to produce GEN3 was not used in this study. In view of the similarities in composition and microstructure between TRIP and GEN3 steels, the TRIP steel heat treatment was chosen for ease, and intended to produce a microstructure consisting of fine-grained ferrite, carbide-free bainite, martensite, and retained austenite. GEN3 steels also show similar microstructure but with a higher amount of retained austenite of around 15% or higher. GEN3 steel can be considered as specialized TRIP steel as it contains both retained austenite and silicon. The annealed panels were electrogalvanized in the laboratory in an electrolytic recirculating cell. After treatment in the CAL, simulator panels were trimmed to 220×160 mm for plating. The laboratory recirculating electrolytic cell used for electrogalvanizing is shown in Fig. 4. The electrolyte used was a solution of zinc chloride, and zinc panels were used as anodes. The sample panels acted as the cathodes. Plating thickness was controlled by controlling the current passed through the cell from a rectifier. The aim plating thickness was 60 g/m² per side and the actual average (from five samples) plating weight obtained was 64 g/m². Samples required for welding and Gleeble® testing were cut from these panels.

Base material average tensile properties were determined prior to welding. The amount of retained austenite present was measured in three samples from each heat using the x-ray diffraction method. This is important because, depending on the silicon level present in each heat, the amount of

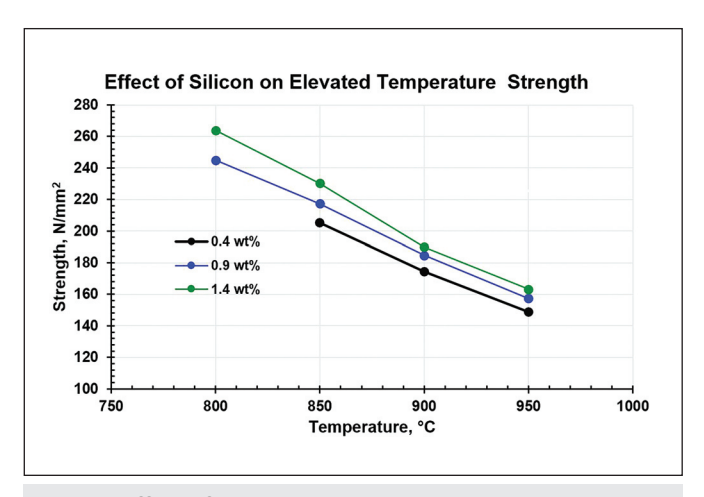


Fig. 7 — Effect of silicon on steel elevated temperature strength.

retained austenite present will likely vary among the heats. Resistance spot welding was done using a Taylor Winfield welding machine with a C-frame powered by an alternating current power source. The welding machine details are provided in Table 2. To assess the effect of silicon on weldability, two tests were done: one was the welding current range determination test, and the other, weld strength determination. Due to limited availability of sample material, weld strength determination was done only at 6√t weld size, where t is the nominal sheet thickness. The current required to produce this weld size was obtained from the current range determination test. Welding current range determination and weld tensile tests were done per Ref. 20. Samples were welded using RWMA Type 2 copper chrome electrodes. Welding conditions used are shown in Table 3.

Weld samples from the welding current range determination were prepared for an examination using an optical as well as a scanning electron microscope equipped with an energy-dispersive x-ray spectrometer. Weld samples from the current range tests were first examined using the dyepenetrant test (DP). No clear DP indications were found in welds. The welds were later cross sectioned perpendicular to the longitudinal axis of the peel samples. Samples were examined for the presence of LME cracks. Number of cracks, maximum crack length, and cumulative crack length were determined for all three heats at each welding current. Three weld shear-tension and cross-tension tests were performed from each heat.

Hot tensile testing was done using a Gleeble® 3500 system. Gleeble® is a thermomechanical simulator that is quite useful in studying weld phenomena. It is capable of rapid heating and cooling rates to simulate weld phenomena. Reduced cross-section, dog-bone-shaped samples were used for Gleeble® testing — Fig. 5. For the tests, samples were heated at 350°C/s to the desired peak temperature, held for a second, and force applied on the sample. After the samples broke, they were allowed to cool to room temperature before removing them from the test chamber. The heat up rate was chosen because it allowed the temperature overshoot from the desired test temperature to be controlled precisely. Typical overshoot from the aim peak was less than 5°C. A longitudinal strain gauge was used during the test to measure

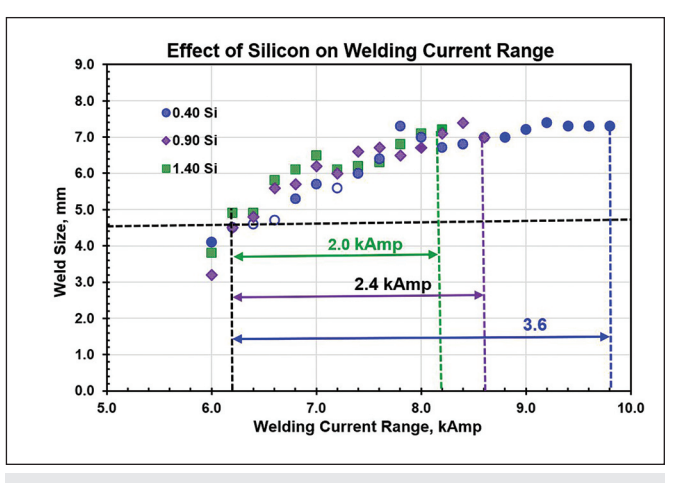


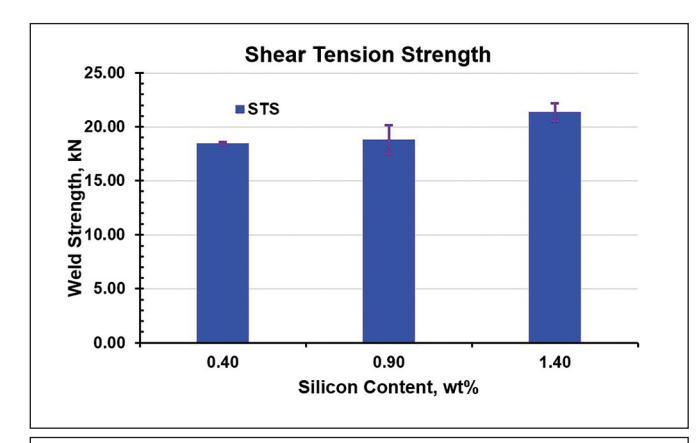
Fig. 8 — Effect of silicon on the welding current ranges.

sample extension more precisely by minimizing slack that can affect the displacement recorded if measurements are taken from clamping jaws. Samples were pulled at a rate of 50 mm/s. All samples were tested in air. Force-displacement curves were obtained from the tests. Tested Gleeble® samples were sectioned along the sample longitudinal axis, mounted, and polished for a metallographic examination using an optical and a scanning electron microscope. At each peak temperature both bare (plating stripped) and electrogalvanized samples were tested.

Electron backscattered diffraction (EBSD) work was done on both the base materials and weld areas with cracks. A JEOL JSM 6610-LV scanning electron microscope equipped with an Oxford energy-dispersive x-ray spectrometer and EBSD was used. Grain boundary characterization and determination of fraction of coincidence site lattices (CSL) of different types were performed.

As silicon levels were varied, the amount of retained austenite was expected to vary among the three heats. To determine if the presence of retained austenite in steel is a prerequisite for LME cracking to occur, a commercial heat of 980GEN3 steel electrogalvanized with 60 g/m² coating weight per side was used. The composition of the commercial heat was identical to that of Heat C with the same silicon level. The use of a commercial heat was necessitated due to the shortage of laboratory-produced material.

Tensile properties of the base material were first determined using the Gleeble® samples. Using this tensile data, Gleeble® samples were strained to different levels in a tensile testing machine and removed. The prestrained samples were checked using the x-ray diffraction method for the amount of retained austenite present after prestraining. After determining the strain required to transform retained austenite to martensite from the prestrained samples, Gleeble® samples were then strained to this level. An x-ray diffraction test confirmed the prestrained samples had no measurable retained austenite. After prestraining, examination under a stereoscope confirmed that prestraining did not compromise the plating layer integrity on the Gleeble® samples. The galvanized plating was stripped from five Gleeble® samples by immersing them in hydrochloric acid. These bare (no electrogalvanized layer) samples were also prestrained to the same degree as the electrogalvanized prestrained samples. Verification using the x-ray dif-



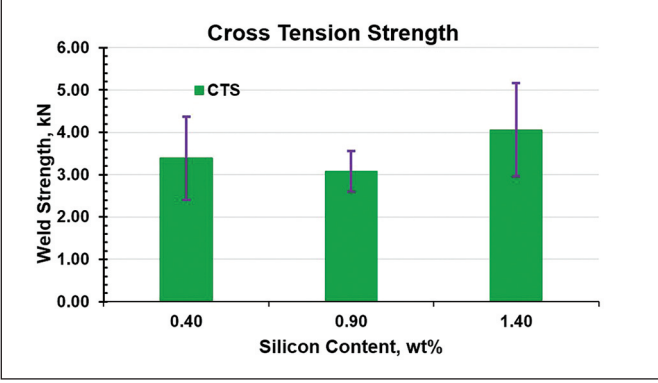


Fig. 9 — Effect of silicon on the weld shear (top) and crosstension (bottom) strength.

fraction method on the prestrained bare samples confirmed that there is no measurable retained austenite. The prestrained bare samples (zinc plating stripped) were tested to-compare the results to those from prestrained electrogalvanized samples. To benchmark the Gleeble® test results from prestrained electrogalvanized and bare samples, nonprestrained bare and electrogalvanized samples were also tested.

Results

Weldability Evaluations

The tensile properties determined from uncoated samples for the three silicon levels are shown in Fig. 6. It is apparent from this figure that increasing silicon content increased base material tensile strength. The most notable effect of silicon is in increasing the elongation of the base materials. Note that GEN3 steels show higher total elongation in the range of 20 to 22% due to a higher amount of retained austenite present compared to the laboratory heats that were heat treated to produce TRIP microstructure. The retained austenite measurements on the base materials are shown in Table 4 and contribute to the higher total elongation observed in the higher silicon base materials. The tensile strength of the base materials in the bare condition determined from the Gleeble® samples shows that higher silicon heat retained higher strength even at higher temperatures — Fig. 7. The data shown in Fig. 7 is for comparison purpose only as the tensile samples used in the Gleeble® tests were nonstandard.

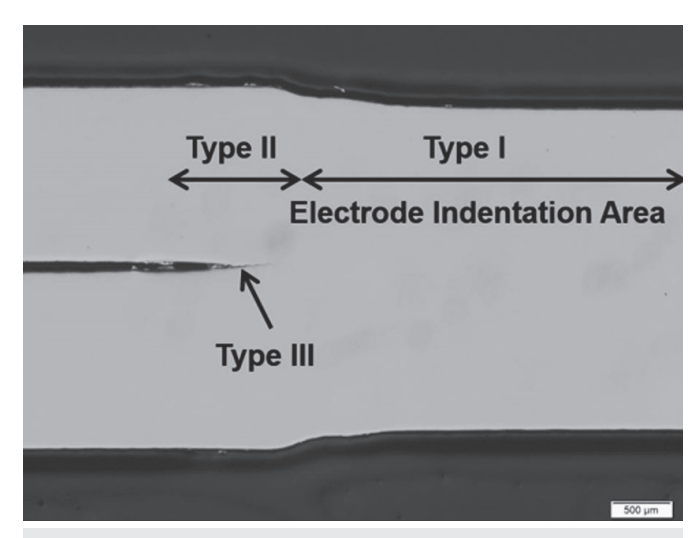


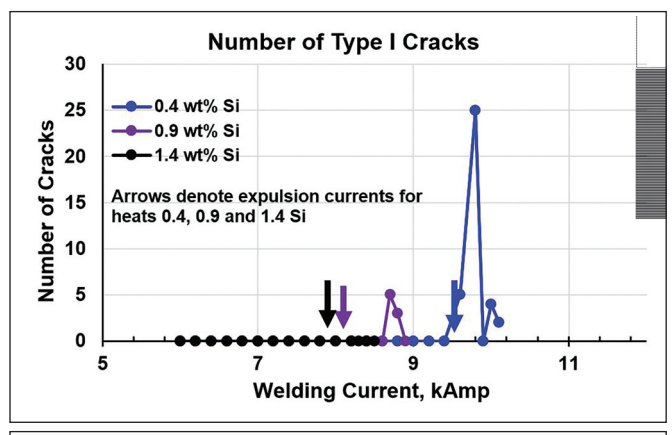
Fig. 10 — Weld cross section showing the regions of a weld for classification of LME cracks.

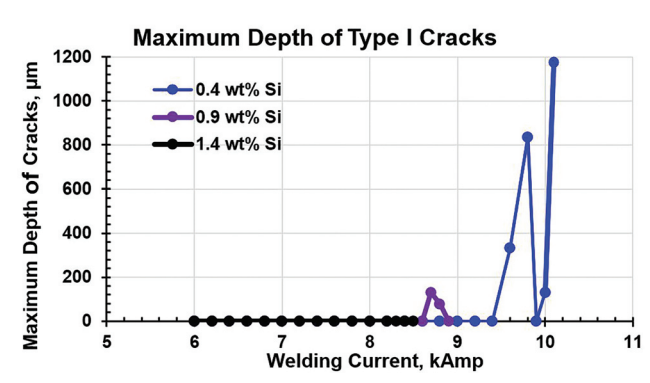
The welding current ranges determined are shown in Fig. 8. This plot shows that increasing silicon content of the steel decreased the welding current range. Welding current range is the useful current window, meaning any welding current chosen within this window produces acceptable weld sizes from a minimum weld size of $4\sqrt{t}$, where t is the nominal sheet thickness, and expulsion weld size. At and beyond expulsion current, the excessive heat input results in expulsion of weld metal, which can result in lowering of the weld size and strength. The use of $4\sqrt{t}$ weld size for the minimum weld size is generally accepted in the automotive industry.

Weld shear and cross tension strengths at various silicon levels are shown in Fig. 9. The data indicates there is not much difference between heats A (0.4% silicon) and B (0.9% silicon), but heat C (1.4% silicon) showed a noticeable improvement in both shear and cross-tension strengths within the scatter observed.

LME Evaluations

Cracks found in weld samples were classified into three types. Type I cracks are those that were found under the electrode indentation, Type II are those that occurred outside the electrode indentation to the heat-affected zone (HAZ), and Type III are those found at the sheet-to-sheet interface. A weld cross section showing these crack locations is shown in Fig. 10. Figures 11 and 12 show the crack features such as their number, maximum crack length, and cumulative crack length for crack Types I and II. Examination did not clearly reveal any cracks that could be identified as Type III. Only at very high magnifications greater than 400× were faint Type III cracks seen in welds from Heat C. In some samples at low welding currents, zinc penetration was observed to occur into the gap between the sheets and appeared like zigzag cracks. These were not counted as cracks. Generally, Type III cracks tend to go up or down from the sheet interfaces either into the fusion zone or HAZ. Some, on the other hand, propagate along the sheet-to-sheet interface. These can be clearly distinguished from incomplete fusion as they tend to have a slight zigzag path. Incomplete fu-





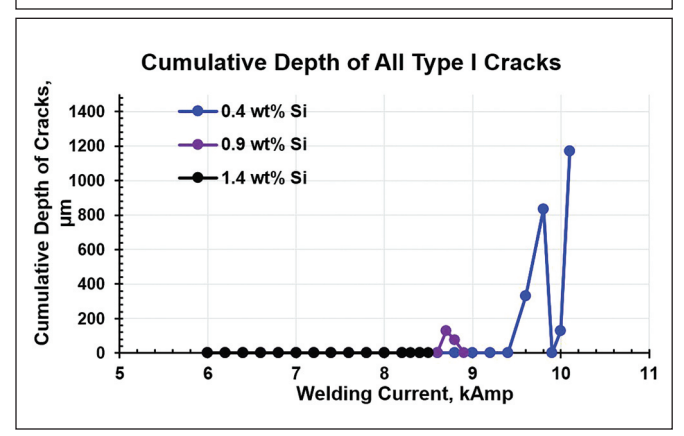
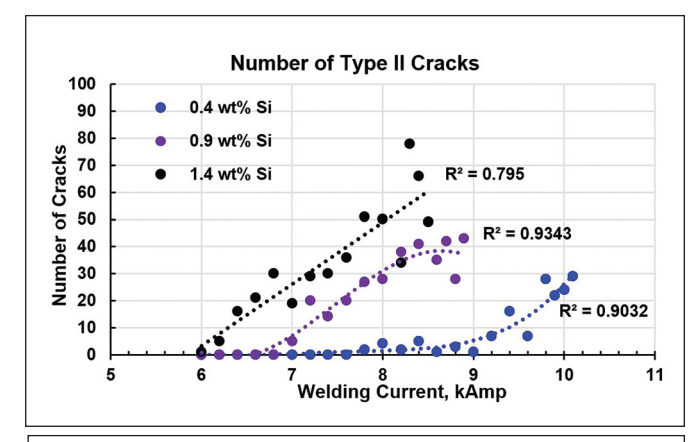


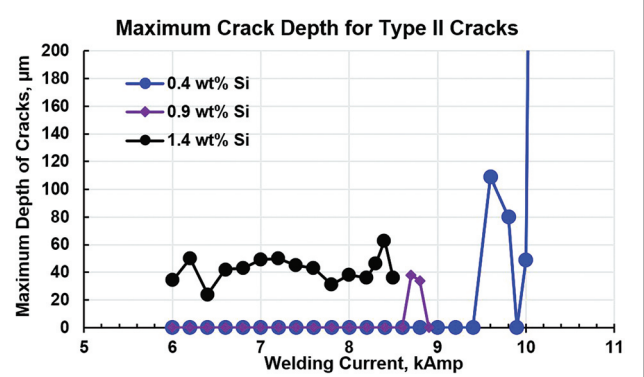
Fig. 11 — Plots showing the number, maximum length, and cumulative lengths of Type I cracks.

sion, on the other hand, tends to be straight.

Gleeble® Evaluations

Plots were made from the Gleeble® force-displacement data obtained. Figure 13 shows typical plots obtained for the three heats at 850° and 900°C aim peak test temperatures. From these data, peak forces were obtained. Up to the point where peak force is reached, numerous small cracks initiate and grow at a slow pace. After peak load is reached, one of these small cracks becomes unstable and starts to propagate catastrophically. From this point onward, the load required for further crack propagation drops. The peak load thus separates the crack initiation stage from the propagation stage. Energies to peak force (crack initiation stage) and





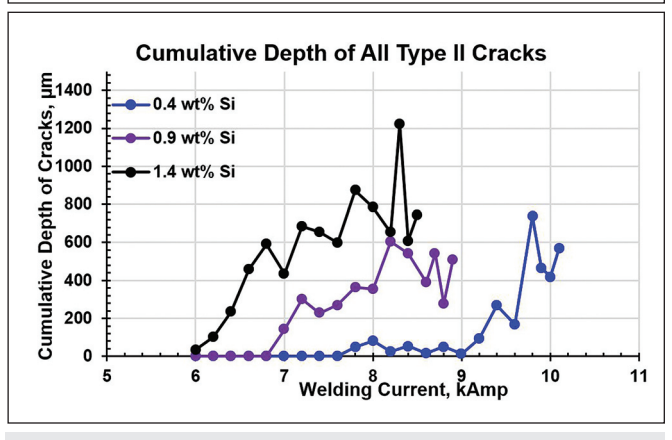


Fig. 12 — Plots showing the number, maximum length, and cumulative lengths of Type II cracks.

post peak force (crack propagation stage) were calculated from the force-displacement data. It may be seen in Fig. 13 that the bare sample from heat C shows high stiffness (slope of force vs. displacement). This behavior is not typical and has never been seen before nor after this one sample. It is suspected that this anomalous behavior is due to the stiffness of the grips that hold the samples in the Gleeble®, which for some unknown reason didn't show displacement properly. This manifested as a steep rise in load without the typical displacement. Examination of the energy absorbed by the bare sample at 900°C was consistent with the trend seen in energy absorption of bare samples at various temperatures. Therefore, the observed stiffness in this one sample did not influence the results and is of no consequence.

Plots were made of the difference in the peak force re-

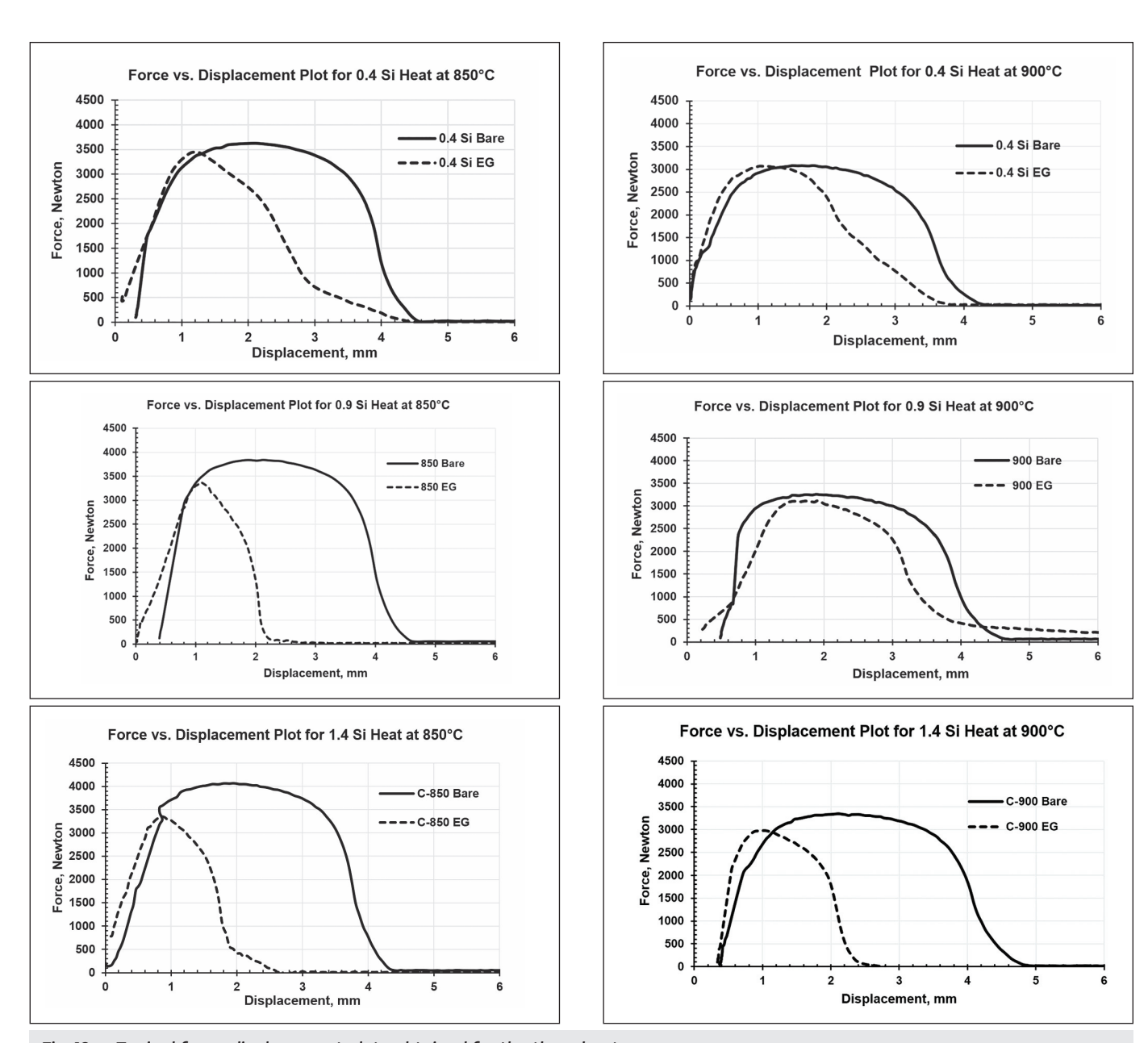


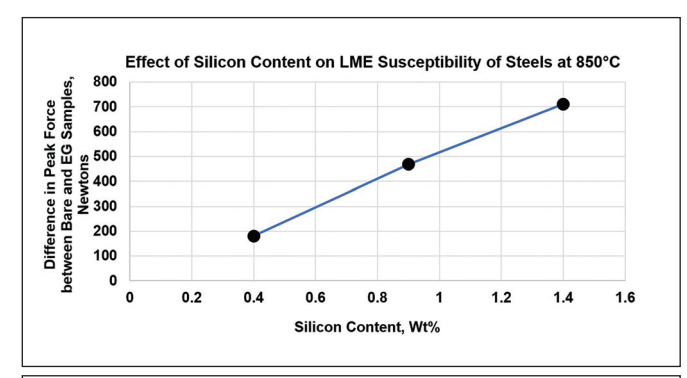
Fig. 13 — Typical force-displacement plots obtained for the three heats.

quired for crack initiation between bare and electrogalvanized samples at each test temperature. These are shown in Fig. 14. The higher the difference in the peak force required for crack initiation between bare and electrogalvanized (EG) samples, the higher is the steel's propensity to LME cracking in electrogalvanized (EG) samples. Figure 15 shows the summary of the differences in the peak loads required between bare and EG samples at all test temperatures. It is interesting to note that both 0.4 Si at all test temperatures and 0.9 Si heat at the highest tested temperature showed a negative difference between bare and (EG) samples, indicating that the EG samples required higher force for crack initiation than the bare samples.

Results indicate that beyond 900° and 925°C LME — as indicated by the difference in peak load between bare and EG samples and the energy absorbed during Gleeble® testing — disappeared for the 0.4- and 0.9-Si heats, respectively. This is

evident based on the results that the EG samples from these two heats did not require lower forces for failure compared to those from bare samples. Even though some LME cracks were still present in EG samples in 0.4 and 0.9 Si heats at 900° and 925°C, they did not propagate catastrophically leading to lower force for failure nor decreased energy absorption. Zinc evaporates around 900°C. The observation that small LME cracks were seen in EG samples at 900° and 950°C indicates that, despite the rapid heating rate used, some molten zinc appeared to have entered the substrate leading to cracking. However, the extent of cracking diminished at and beyond 900°C. After 950° and 1000°C, no difference in the peak forces (in the forcedisplacement curve) were seen between bare and EG samples. Because for LME to occur, the presence of liquid zinc is required, the rapid evaporation of zinc might have alleviated LME-induced cracking.

The 1.4-Si heat showed a broader range of temperatures



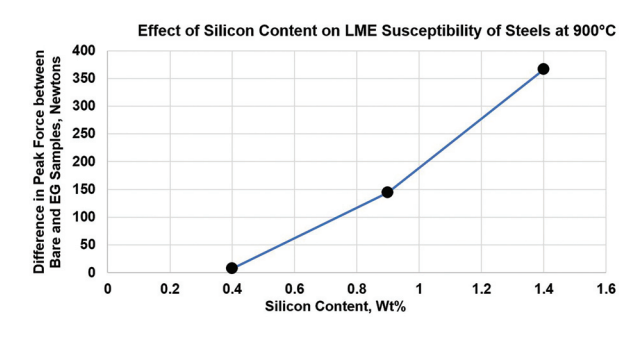


Fig. 14 — Plots showing the effect of silicon on the difference in peak force required for cracking between bare and electrogalvanized samples at 850° and 900°C test temperatures.

from 800° to beyond 950°C, in which it is susceptible to LME cracking. Figure 16 shows the plot between total energy absorbed during the Gleeble® tests for all three heats and the test temperatures. No bare samples were tested for the 0.4-silicon heat due to unavailability of the test material. Figure 17 shows cross-sectional views of Gleeble® samples from all three heats. It can be seen that the amount of necking decreased as the silicon content increased, which indicates that higher silicon samples broke without much plastic deformation.

Effect of Retained Austenite

Figure 18 shows the force-displacement plots for bare and EG samples of 980GEN3 steel before and after prestaining and testing at 850°C. The bare prestrained samples were used to benchmark the performance of prestrained EG samples. The plot clearly shows the peak force differences between bare and EG samples and the prestrained EG samples that had no measurable retained austenite exhibited lowering of peak force required for crack initiation. Figure 19 shows the force-displacement plot for prestrained bare and EG samples tested at 850°C, and Fig. 20 shows cross-sectional views of prestrained bare and EG samples. Further, the amount of necking seen in the prestrained EG sample was much less than that seen in the prestrained bare samples.

Energy absorbed data during the tests were examined when crack initiation occurred (precrack) and when sample failures occurred (crack propagation) — Fig. 21. Results showed prestrained EG samples required much less energy for crack initiation and propagation compared to prestrained bare samples, a conclusion that is attributed to

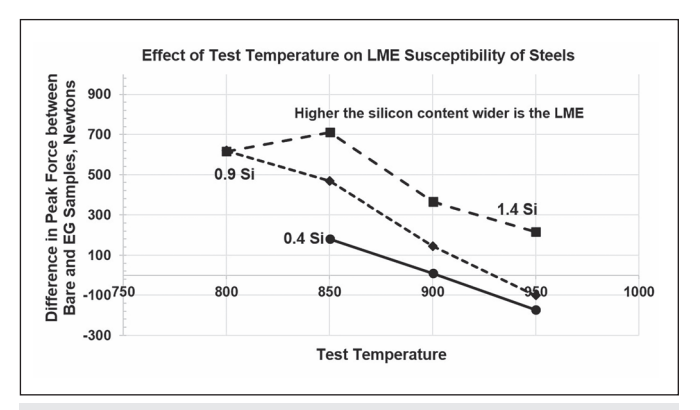
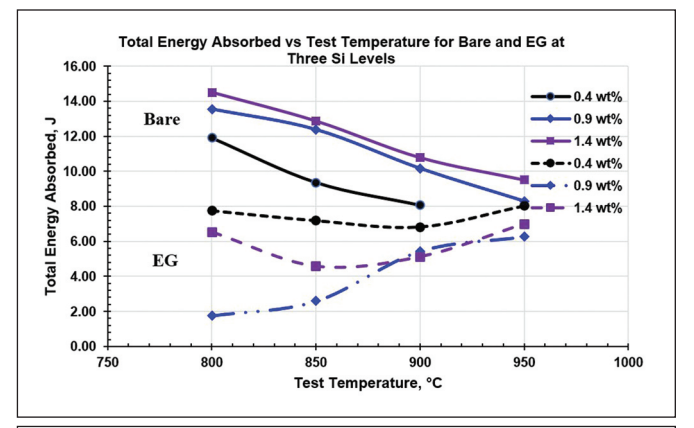


Fig. 15 — Plot of differences in the peak force required between bare and EG samples. Negative difference for the 0.4-Si heat indicates EG samples required higher force to initiate cracks than bare samples.



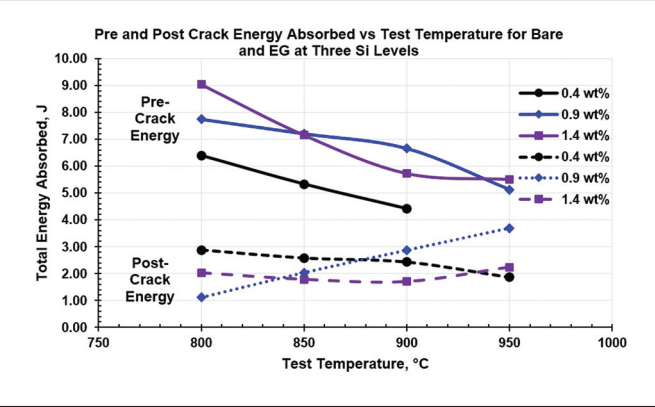


Fig. 16 — Plot between total energy absorbed (top) and preand postcrack energies absorbed during Gleeble® tests between bare and EG samples at each test temperature. Solid lines represent bare samples and dashed lines represent EG samples (top). Solid lines in the bottom plot represent precrack and dashed lines represent postcrack energies.

the presence of LME cracks. This means prestrained EG samples that did not contain any measurable retained austenite exhibited embrittlement from LME cracking.

EBSD Results

The inverse pole figures and image quality maps with

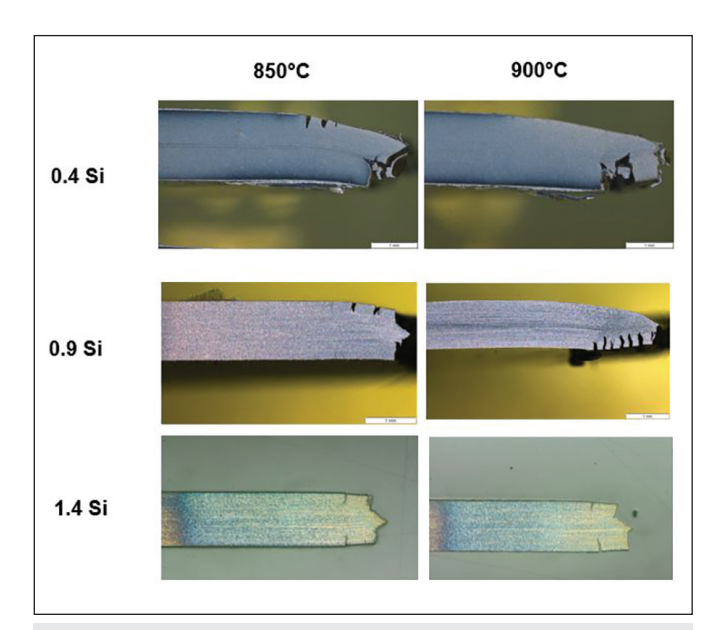


Fig. 17 — Cross-sectional views of Gleeble® samples showing LME cracks. Some amount of necking can be seen in 0.4-and 0.9-silicon heats.

grain boundary maps overlaid for the three heats and welds are shown in Figs. 22 and 23, respectively. A summary of the grain boundary character distribution (GBCD) plot is shown in Fig. 24. From these data, it appeared the GBCD was essentially similar among all three base materials. However, differences can be seen in the GBCD in the weld areas — Fig. 24. Heat A showed a relatively higher fraction of low angle boundaries, and a smaller fraction of high angle boundaries compared to the other two heats. Heat C showed a higher fraction of high angle boundaries compared to heats B and C. Differences were noted in the CSL boundary distribution among the heats. Examination of the CSL data (Fig. 25) from the base materials and weld area shows that the fraction of Σ 3 boundaries decreased as the silicon content of the steel increased.

Discussion

Silicon Effect on Cracking

Silicon has a strong effect on the bulk resistivity of steel. Therefore, increasing silicon content causes more resistive heat to develop during welding, which leads to early expulsion of weld metal at relatively low welding currents compared to low-silicon steels. This causes the useful current range to decrease when the silicon level of steel goes up. Interestingly, the welding current required to obtain the minimum weld size is the same for all three heats. One explanation for this is that the weld sizes that exceeded $4\sqrt{t}$ weld size were different. For 0.4- and 0.9-silicon heats, the minimum weld sizes achieved were 4.7 and 4.8 mm, and the minimum weld size required is 4.7 mm. However, at the same welding current, the minimum weld size achieved for the 1.4-silicon heat was 5 mm. This means the same welding current produced different weld sizes in the three heats, and the weld sizes increased as the silicon con-

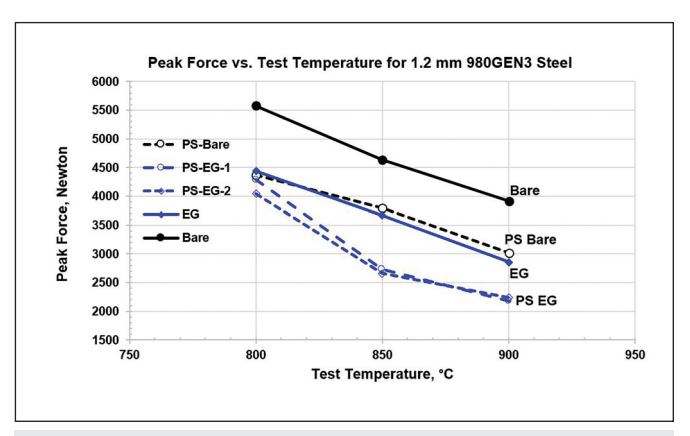


Fig. 18 — Plot of peak force and test temperature for bare, electrogalvanized (EG), prestrained bare (PS-bare), and prestrained electrogalvanized (PS-EG-1 and PS-EG-2) samples of 980GEN3 steel.

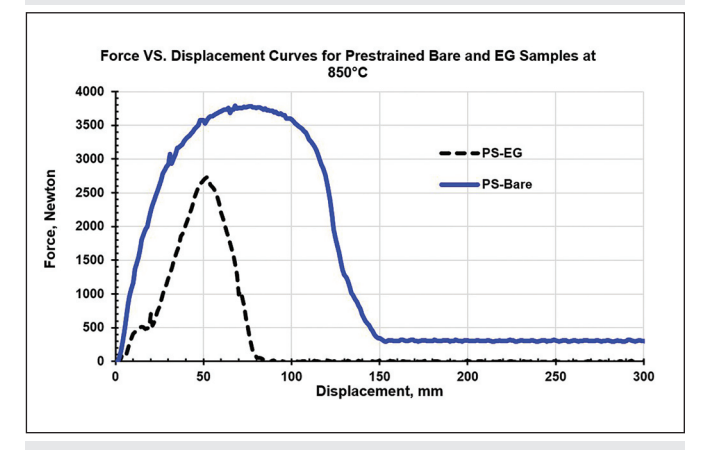


Fig. 19 — Force-displacement plot for prestrained bare and EG samples tested at 850°C.

tent went up. Silicon increases bulk resistivity of steel and is believed to be the reason for obtaining larger weld sizes as silicon content went up.

Previous researchers have used a more extensive classification of cracks to examine the causes for their origin (Refs. 10, 17). In this study, for simplicity and ease of explanation, cracks observed in welded samples were classified into three types. The crack numbering used is arbitrary and is intended to identify the possible cause of cracking. Cracks shallower than 10 µm were ignored as insignificant for the count. Type I cracks formed above expulsion currents in all heats. Type I cracks did not seem to be composition dependent, but rather welding current dependent. When the welding current exceeded 200 A above expulsion current, cracks as deep as 1 mm were found in the welds. These results suggest Type I cracks can be avoided only if high currents that lead to weld expulsion are avoided. Higher silicon seems to promote more Type II cracks even at low welding currents. Further, most of the cracks observed in the 1.4-Si heat were around 40 μm or deeper. Both 0.4- and 0.9-Si heats showed no Type II cracks until expulsion current was reached. In the 0.9-Si heat, there were numerous cracks around 8 kA, but they had no significant depth to them. It can be seen from Fig. 11 that the cumulative depths for cracks was higher as

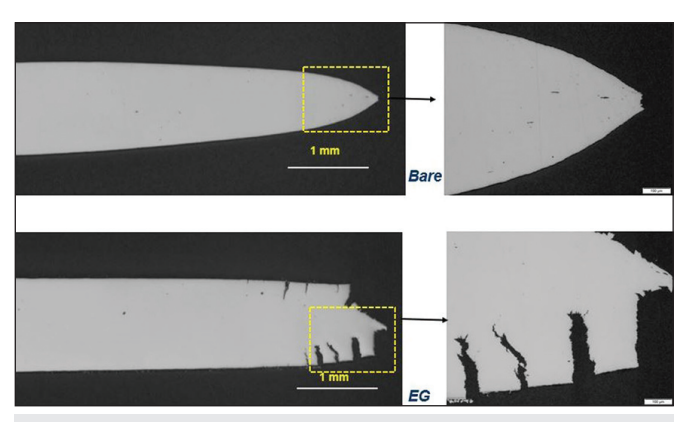


Fig. 20 — Cross-sectional views of prestrained bare and EG Gleeble $^{\circ}$ samples tested at 850°C showing cracks in the EG samples.

silicon content in the steel increased. At the expulsion current, cracking in welds was aggravated and increased not only Type I but Type II cracks as well. These observations underscore the need to use appropriate welding current to minimize weld metal expulsion from high heat input. High heat input in welding results from the use of high welding current. The absence of any Type III cracks is not surprising as these cracks are induced typically by misorientation between base materials to be welded and welding guns (Ref. 19). Thus, Type I and Type III cracks were labeled as manufacturing-related LME cracks, and can occur in any steel if welding conditions, such as heat input and alignment or orientation of welding electrodes to base materials, are not properly controlled (Ref. 19).

Gleeble® studies showed similar results regarding the effect of silicon on LME cracking as those seen with welding studies. Results indicates that beyond 900° and 925°C, LME as indicated by the difference in peak forces between bare and EG samples as well as energy absorbed in Gleeble® testing disappeared for 0.4 and 0.9 heats, respectively. However, in comparison, the 1.4-Si heat showed a broader range of temperatures from 800° to beyond 950°C, in which it is susceptible to LME cracking. The practical significance of this observation is that avoiding LME cracking by using lower welding heat input in the 1.4-Si heat is extremely difficult because of the broad temperature range over which LME cracking can occur. Lowering the heat input either by using lower welding current or shorter time of welding increases the welding cooling rates and is expected to narrow the weld HAZ. This means the width of the HAZ over which LMEsusceptible temperature can occurs narrowed. However, for the 1.4-Si heat, as the LME-susceptible temperature range is broad, avoiding LME cracking using heat input control during welding is a difficult proposition.

Energy absorption differences between bare and EG samples diminished beyond 900°C for 0.4- and 0.9-Si heats — Fig. 13. The 1.4-Si heat showed significant loss of energy absorption in electrogalvanized samples even at 950°C, indicating brittle behavior due to LME cracking. Thus, it is apparent that the energy absorption results are consistent with those of peak force differences between bare and electrogalvanized samples observed at various temperatures. Higher silicon seems to promote brittle behavior due to

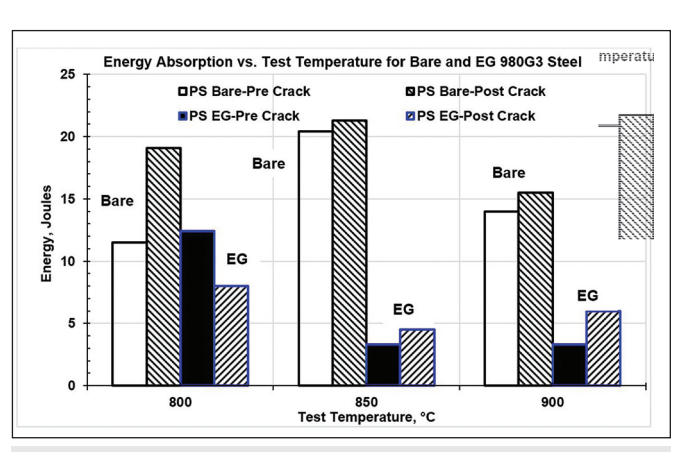


Fig. 21 — Plot of energy absorption in bare and electrogalvanized (EG) samples.

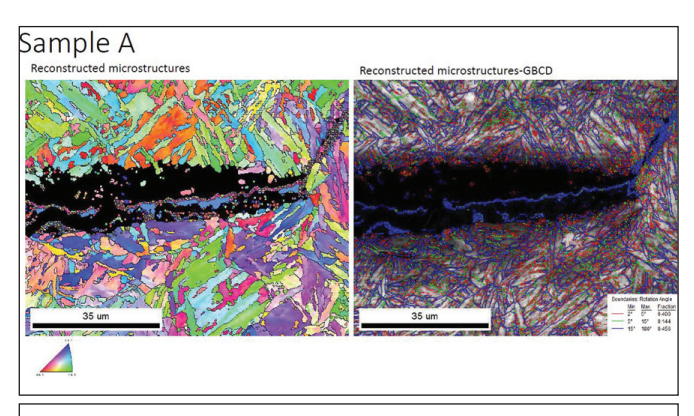
LME over a wide range of temperatures and suggests LME cracking avoidance for the 1.4-Si heat is difficult.

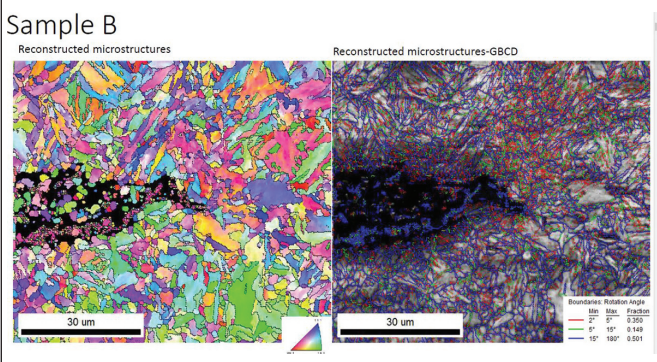
The need to achieve the required strength-elongation properties and produce a steel with acceptable LME cracking resistance has to be balanced in high-strength steels, including GEN3 steels. Based on the present results, it appeared that silicon should be kept below 0.9 wt-%. At 0.4 wt-% silicon, there was no measurable retained austenite in the microstructure, and elongation of the base material was low. While there was some improvement in the tensile properties at 0.9 wt-% silicon, the LME performance was moderate. So, it appears that silicon levels around 0.6 to 0.8 wt-% might strike a balance between achieving the required properties and managing LME performance of the steel. The latter one is important from the steel end user standpoint. To achieve the required minimum elongation for a GEN3 steel, the amount of retained austenite has to be doubled from that seen in the 1.4-silicon heat. However, the composition requirements have to be carefully considered depending upon various other processing needs.

Effect of Silicon on Grain Boundaries

Grain boundary engineering (GBE) deals with practices to obtain materials with grain boundaries that have desirable properties. One desirable property that has been the focus of GBE is the resistance to crack propagation in materials. Desirable properties in terms of crack resistance are associated with boundaries with simple, low-energy structures as studies have shown that low angle boundaries resist cracking (Ref. 21). Low-energy, simple structures are associated with coincidence site lattice (CSL) boundaries. Although we now know that certain grain boundaries have desirable properties (specifically in face-centered cubic metallic systems), information on the paths to produce such structures is lacking.

The extent of the fit between two adjacent grains is characterized by the reciprocal of the ratio of the number of coincidence sites to the total number of sites. This is expressed by the Σ number. Grain boundaries with different Σ numbers have different properties. Σ 3 boundaries are reported to be low-energy boundaries with a high resistance to impurity segregation (Ref. 21). Further, it was reported that low angle (Σ 1)





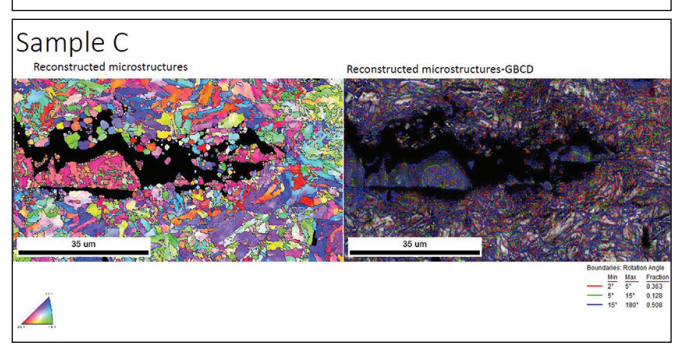
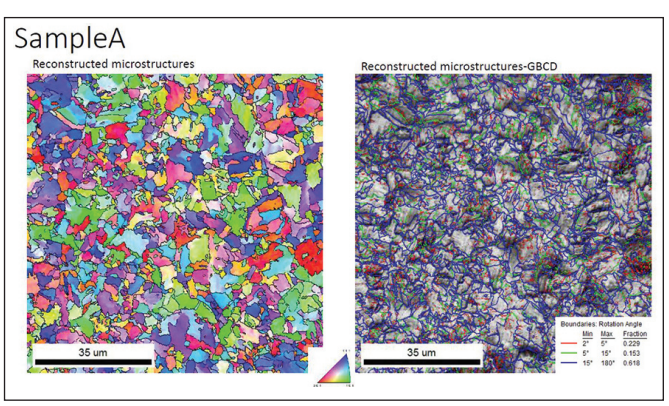
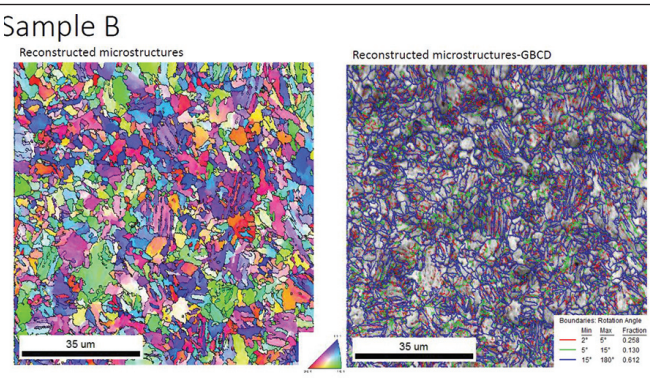


Fig. 22 — Maps showing inverse pole figures and image quality with grain boundary distribution overlaid on the microstructure for the three heats in the weld area near LME cracks.

and symmetrical $\Sigma 3$ boundaries were particularly strong, and all high angle boundaries, regardless of their Σ values, were weak. It was found that even low- Σ CSL boundaries, if their misorientation was high (generally higher than 15 deg), were found to be weak sites and preferred paths for intergranular crack propagation (Ref. 22). The presence of increasingly higher fraction low angle $\Sigma 3$ boundaries as silicon content of the steel was decreased may explain the reason for improved resistance to LME cracking as the silicon content was lowered.

Studies on grain boundary structure and misorientation in weld metals have been limited. Two such studies that characterized grain boundary structure in single-phase weld metals were published by Lippold and co-workers (Refs. 23, 24). These authors classified grain boundaries in weld metals into three groups, namely the solidification grain boundaries (SGBs), solidification subgrain boundaries (SSGBs), and migrated grain boundaries (MGBs). The MGBs are not clearly distinguishable in alloy systems that solidify into multiple phases or mixtures thereof. The SGBs are the high angle boundaries





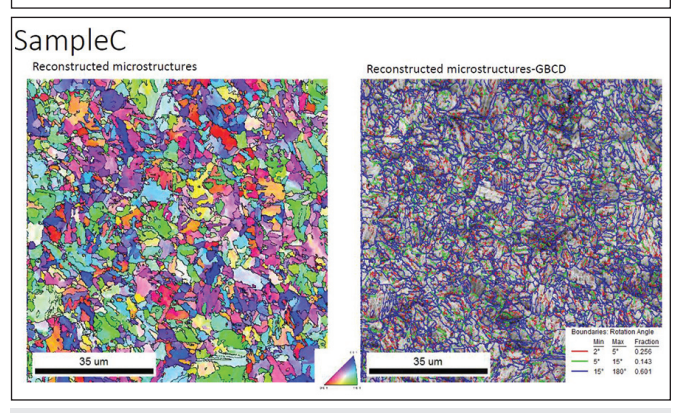
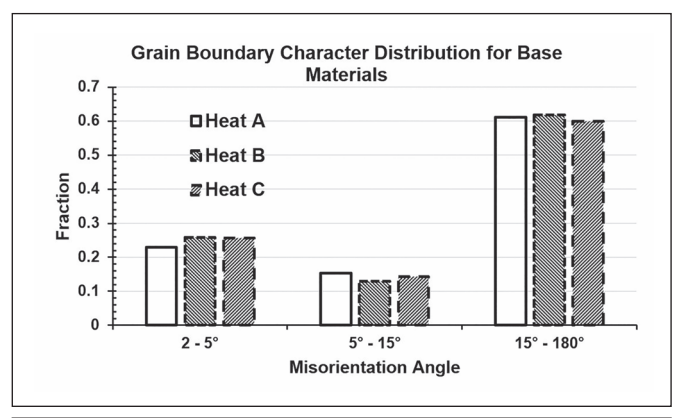


Fig. 23 — Maps showing inverse pole figures and image quality with grain boundary distribution overlaid on the microstructure for the three heats in the base materials.

and are the preferred sites for cracking, such as solidification cracking, to occur in austenitic weldments. The SSGBs are low angle grain boundaries and represent boundaries of various types of solidification modes, such as cells, dendrites, and cellular dendrites. These boundaries have rarely been observed to be crack paths. The presence of higher fraction of low angle boundaries may indicate the relative resistance to crack propagation as silicon content of the steel decreased. This is important because, once surface LME cracks initiate, they very soon encounter the fusion zone as they propagate into the subsurface. Further propagation deep into the weld is likely to be influenced by the types of grain boundaries ahead of the crack path in the weld fusion zone.

Effect of Retained Austenite on LME cracking

The results showing the presence of retained austenite is



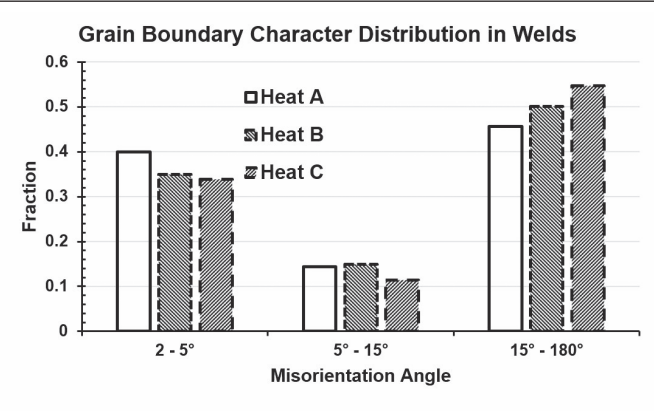


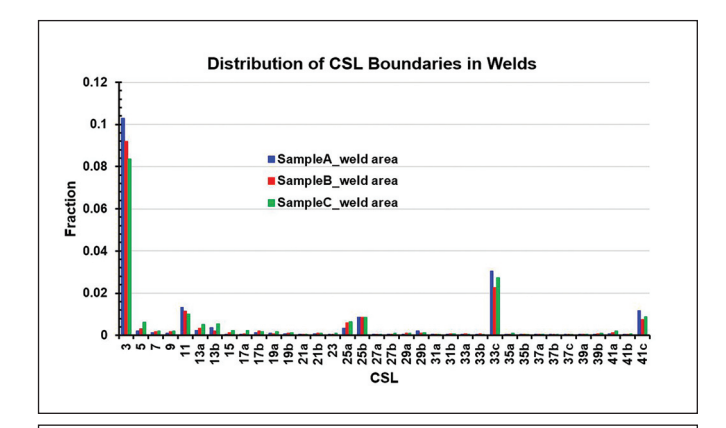
Fig. 24 — Grain boundary character distribution plots for base materials (top) and welds (bottom).

not a prerequisite for LME cracking to occur is not surprising for a couple of reasons. One is steel grades that do not contain retained austenite, such as dual-phase steels, have been found to exhibit LME cracks. The second is temperature in the far and near HAZs gets into the austenitic temperature range of steel. Therefore, austenite is present at welding temperatures regardless of whether the starting microstructure has retained austenite. It is possible TRIP steels that have been reported to exhibit LME cracking contained a significant amount of silicon. Typical silicon level for a 780-MPa TRIP steel is around 1.4 wt-% and is added to stabilize austenite at room temperature. This level of silicon has been shown in the present study to increase LME susceptibility of the steel.

Conclusions

The following conclusions can be drawn based on this study:

- 1. Increasing silicon in steel seemed to provide good high-temperature strength and a small, yet noticeable, increase in weld cross-tension strength. However, increasing silicon lowered the useful welding current range, which is not a desirable feature from a manufacturing standpoint.
- 2. Silicon was found to have a profound effect on the LME cracking behavior of steels that rely on TRIP effect to achieve high elongation. Increasing silicon in the steel seems to promote both Type I and Type II cracks in the weld areas. Some of the Type II cracks were seen even at welding currents well below the weld expulsion currents. In this regard,



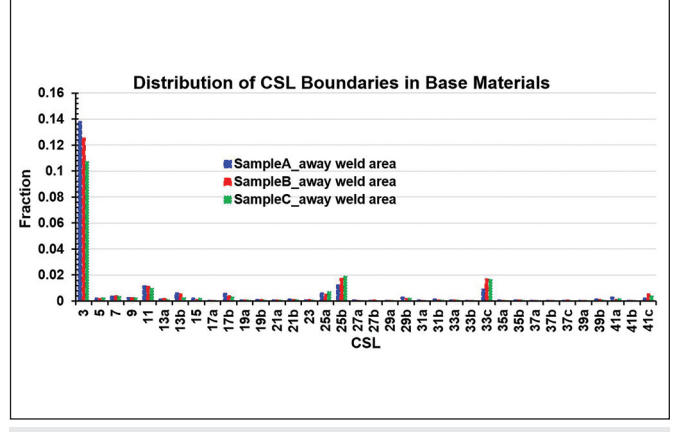


Fig. 25 — CSL distribution comparison in welds (top) and base materials (bottom).

both weld and Gleeble® evaluations showed similar results on the influence of high silicon in promoting LME cracking.

- 3. Increasing silicon content in steel seems to widen the temperature range over which LME cracking can occur. This makes control of LME cracking by limiting welding heat input a difficult and challenging task.
- 4. At lower silicon levels, a higher fraction of $\Sigma 3$ CSL boundaries were found in the steel. These CSL boundaries have low energies associated with them and are beneficial from a crack resistance standpoint. At lower silicon levels, the fraction of low angle boundaries was high in welds. The low angle boundaries also have low energy associated with them. These two factors might explain the beneficial role played by lowering silicon in steel.
- 5. It was found that retained austenite is not required in steel for LME cracking to occur. It has been shown in this study that, in retained austenite-containing steels, LME cracking is from the presence of higher amounts of silicon added to retain austenite at room temperature for TRIP effect.

Acknowledgments

The author gratefully acknowledges the help of C. J. Wu and E. A. Silva of this laboratory in melting, rolling, and electroplating of the base materials used in this study. The author is grateful to M. J. Merwin for a critical review of the manuscript and to Prof. Garcia of the Department of Mechanical and Materials Engineering, University of Pittsburgh, for sever-

WELDING RESEARCH

al helpful discussions. Thanks are due to several of the technicians at this laboratory who participated in this two-year research project. Notable among them are E. W. Buterbaugh (formerly of this laboratory) for welding, J. Bryan for Gleeble® work, J. Paulina for mechanical testing, S. Mudron for machining, and J. Vargo, J. F. Bumbernick, and K. Bennethum for metallographic work. Finally, the author would like to thank D. J. Radakovic for reviewing the statistical analysis of the data.

Disclaimer

The material in this paper is intended for general information only. Any use of this material in relation to any specific application should be based on independent examination and verification of its unrestricted availability for such use and a determination of suitability for the application by professionally qualified personnel. No license under any United States Steel Corp. patents or other proprietary interest is implied by the publication of this paper. Those making use of or relying upon the material assume all risks and liability arising from such use or reliance.

References

- 1. Tumuluru, M. 2017. Resistance spot welding of new generation of high strength automotive steels. Invited paper presented at the Trends in Welding Research conference, Tokyo, October 13, 2017.
- 2. Tumuluru, M. 2006. Resistance spot welding coated high-strength dual-phase steels. *Welding Journal* 85(8): 31–37.
- 3. Tumuluru, M. How composition affects weldability of steels. *Welding Journal* 94(6): 72–75.
- 4. Matlock, D. K., and Speer, D. J. 2006. Design considerations for the next generation of advanced high strength sheet steel. *Proceedings of the Third International Conference on Structural Steels, H. C. Lee, ed.* The Korean Institute of Metals and Materials, Seoul, pp. 774–781.
- 5. Wang, L., and Speer, J. 2013. Quenching and partitioning steel heat treatment. *Metallography, Microstructure and Analysis* 2: 268, 281
- 6. Stoloff, N. S. 1968. Liquid metal embrittlement. In: Burke, J. J., Reed, N. L., and Weiss, V. (eds.) *Surfaces and Interfaces II. Sagamore Army Materials Research Conference Proceedings*, Vol. 14. Springer, Boston. Mass.
- 7. Stoloff, N. S., and Johnston, T. L. 1963. Crack propagation in a liquid metal environment. *Acta Met*. 11: 251–256.
- 8. Beal, C., Klebera, D., Fabreguea, D., and Bouzekrib, M. 2012. Liquid zinc embrittlement of a high manganese-content TWIP steel. *Material Science and Engineering* Vol. A 543, pp. 76–83.
- 9. Kang, H., Cho, L., Lee, C., and De Cooman, B. C. 2016. Zn penetration in liquid metal embrittled TWIP steel. *Metallurgical and Materials Transactions A* 47(6): April.
- 10. Choi, D.-Y., Sharma, A., Uhm, S.-H., and Jung, J. P. 2018. Liquid metal embrittlement of resistance spot welded 1180 TRIP steel: Effect of electrode force on cracking behavior. *Met. Mater. Int.* DOI: 10.1007/s12540-018-0180-x

- 11. Bhattacharya, D. 2018. Liquid metal embrittlement during resistance spot welding of Zn-coated high-strength steels. *Mater. Sci. Technol.*: 1–21. DOI: 10.1080/02670836.2018.1461595
- 12. DiGiovanni, C., Biro, E., and Zhou, N. Y. 2018. Impact of liquid metal embrittlement cracks on resistance spot weld static strength. *Sci. Technol. Weld. Join.* DOI: 10.1080/13621718.2018. 1518363
- 13. Kim, Y. G., Kim, I. J., Kim, J. S., Chung, Y., and Choi, D. U. 2014. Evaluation of surface crack in resistance spot welds of Zn-coated steel. *Materials Transactions* 55(1): 171–175.
- 14. Lee, H., Jo, M. C., Sohn, S. S., Kim, A-H., Song, T., Kimm, S.-K., Kim, H. S., Kim, N. J., and Lee, S. 2019. Microstructural evolution of liquid metal embrittlement in resistance-spot-welded twinning-induced plasticity (TWIP) steel sheets. *Material Characterization* 147(2019): 233–241.
- 15. Pfestorf, M. 2005. The application of multiphase steel in the body-in-white. Paper presented at the Great Designs in Steel, Steel Market Development Institute (SMDI) of the American Iron and Steel Institute (AISI).
- 16. Wintjesi, W., DiGiovanni, C., Biro, E., and Zhou, N. 2019. Quantifying the link between crack distribution and resistance spot weld strength reduction in liquid metal embrittlement susceptible steels. *Welding in the World* (a publication of the International Institute of Welding). DOI: 10.1007/s40194-019-00712-5
- 17. DiGivonni, C., Han, X., Biro, E., and Zhou, N. Y. 2019. Experimental and numerical analysis of liquid metal-embrittlement crack location-experimental and numerical analysis of liquid metal embrittlement crack location. *Journal of Materials Engineering and Performance*. DOI: 10.1007/s11665-019-04005-2
- 18. Tumuluru, M. 2017. Evolution of generation 3 automotive steels and some studies on their weldability behavior. Paper presented at the International Welding and Joining Conference, Gyeongju, Korea. Korean Welding Society, Seoul, Korea.
- 19. Tumuluru, M. 2018. Weldability of automotive sheet steels beyond generation 1 advanced high strength steels. Paper presented at the International Conference on Advanced Steels, The Korean Institute of Metals and Materials, Geju, Korea. November 18-21.
- 20. AWS D8.9M-2012, Test Methods for Evaluating the Resistance Spot Welding Behavior of Automotive Sheet Steel Behaviors. Miami, Fla.: American Welding Society.
- 21. Gertsman, Y. V., and Bruemmer, S. M. 2001. Study of grain boundary character along intergranular stress corrosion crack paths in austenitic alloys. *Acta Materialia* 49(9): 1589–1598.
- 22. Lin, H., and Pope, D. P. 1993. The influence of grain boundary geometry on intergranular crack propagation in $\rm Ni_3Al$. *Acta Metallurgica et materialia* Vol. 41, pp. 553–562.
- 23. Tumuluru, M., Clark, W. A. T., and Lippold, J. C. 1991. An investigation of boundary structure and composition in single-phase weld metals. *Proceedings of the TMS Fall Meeting*, Cincinnati, Ohio, Oct. 22, 1991.
- 24. Lippold, J. C., Clark, W. A. T., and Tumuluru, M. 1992. An investigation of weld metal interfaces. *The Metals Science of Joining*, Eds.: Cieslack, M. J., Perepezko, J. H., Kang, S., and Glicksman, M. E. The Minerals, Metals, and Materials Society.

MURALI TUMULURU (mtumuluru@gmail.com)